The Molecular Mechanism of Alternative P450-Catalyzed Metabolism of Environmental Phenolic Endocrine-Disrupting Chemicals

Ji, Li; Ji, Shujing; Wang, Chenchen; Kepp, Kasper Planeta

Published in:
Environmental Science and Technology

Link to article, DOI:
10.1021/acs.est.8b00601

Publication date:
2018

Document Version
Peer reviewed version

The Molecular Mechanism of Alternative P450-Catalyzed Metabolism of Environmental Phenolic Endocrine-Disrupting Chemicals

Li Ji[*1,2], Shujing Ji[1], Chenchen Wang[1], Kasper P. Kepp*[*3]

[1] College of Environmental and Resource Sciences, Zhejiang University, Hangzhou 310058, China

[2] UFZ Department of Ecological Chemistry, Helmholtz Centre for Environmental Research, Permoserstrasse 15, 04318 Leipzig, Germany

[3] DTU Chemistry, Technical University of Denmark, Building 206, Kgs. Lyngby, DK-2800, Denmark

Abstract

Understanding the bioactivation mechanisms to predict toxic metabolites is critical for risk assessment of phenolic endocrine-disrupting chemicals (EDCs). One mechanism involves *ipso*-substitution, which may contribute to the total turnover of phenolic EDCs, yet the detailed mechanism and its relationship with other mechanisms are unknown. We used density functional theory to investigate the P450-catalyzed *ipso*-substitution mechanism of the prominent xenoestrogen bisphenol A. The *ipso*-substitution proceeds via H-abstraction from bisphenol A by Compound I, followed by essentially barrierless OH-rebound onto the *ipso*-position forming a quinol, which can spontaneously decompose into the carbocation and hydroquinone. This carbocation can further evolve into the highly estrogenic hydroxylated and dimer-type metabolites. The H-abstraction/OH-rebound reaction mechanism has been verified as a general reaction mode for many other phenolic EDCs, such as bisphenol analogues, alkylphenols and chlorophenols. The identified mechanism enables us to effectively distinguish between type I (eliminating-substituent as anion) and type II (eliminating-substituent as cation) *ipso*-substitution in various phenolic EDCs. We envision that the identified pathways will be applicable for prediction of metabolites from phenolic EDCs whose fate is affected by this alternative type of P450 reactivity, and accordingly enable the screening of these metabolites for endocrine-disrupting activity.

Introduction

Biotransformation plays a critical role in determining the toxicity of xenobiotics in organisms and has drawn considerable attention as a basis for environmental risk assessment.[1,2] Biotransformation of environmental endocrine-disrupting chemicals (EDCs) is one such example.[3,4] Accurate risk assessment of EDCs requires consideration of bioactivation via biotransformation processes, especially by human cytochrome P450 enzymes (P450), since neglecting these metabolic pathways may lead to undervaluation of their adverse effects on human health, although the metabolism of phenolic chemicals by P450 is minor compared with the glucuronidation pathway under normal circumstances.[3,4] P450 enzymes are a superfamily of monooxygenases distributed through all kingdoms of life, and are responsible for most phase-I biotransformation reactions.[5-9] Some of these conversions produce metabolites that are much more toxic than their parent compounds, an important example being phenolic EDCs.[10] Phenolic EDCs such as bisphenol analogues, alkylphenols and chlorophenols, are ubiquitous in the environment as widely used industrial chemicals, with associated high risk of environmental exposure.[10] Among these, although bisphenol A (BPA) has traditionally been considered a weak environmental xenoestrogen because of its much lower binding affinity to the estrogen receptor than that of estradiol,[11] the biotransformation largely affects the endocrine disrupting activity of BPA.[4]

As shown in **Scheme 1**, conjugation with the phase II glucuronide enzyme is the predominant metabolic pathway of BPA in humans (more than 90% of all BPA metabolites), which represents a major detoxification pathway;[12] however, BPA is also metabolized by human P450 to form *ortho*-OH-BPA via hydroxylation of the aromatic ring,[12] to form hydroxycumyl alcohol (HCA), isopropenylphenol (IPP), and hydroquinone (HQ) via an *ipso*-substitution mechanism,[13] and to form a dimer-type metabolite 4-methyl-2,4-bis(4-hydroxyphenyl)pent-1-ene (MBP) whose

formation may involve IPP reacting with isopropenylphenol radical.[14,15] *In vitro* assays have shown that HCA can exhibit 100-fold higher estrogen activity than BPA (concentrations of 10^{-5} to 10^{-10} M),[13] while MBP can be 1000-fold more potent (concentrations of 10^{-5} to 10^{-9} M).[14] Although the *ipso*-substitution pathway of the P450-catalyzed metabolic activation of BPA is most likely a minor pathway under most circumstances, such strong endocrine-disrupting activity of the metabolites makes this pathway important to the overall environmental risk assessment, especially under conditions where glucuronidation is impaired by e.g. other compounds or for genetic or developmental reasons. For example, human fetal livers show little or no glucuronidation[16] and in contrast to rodents express significant levels of P450 leading to metabolizing many xenobiotic compounds even at the prenatal stage.[17,18] thus P450-catalyzed metabolic activation is more likely relatively more significant in the fetus.[3,19,20]

Scheme 1. Major Metabolic Pathways of Bisphenol A

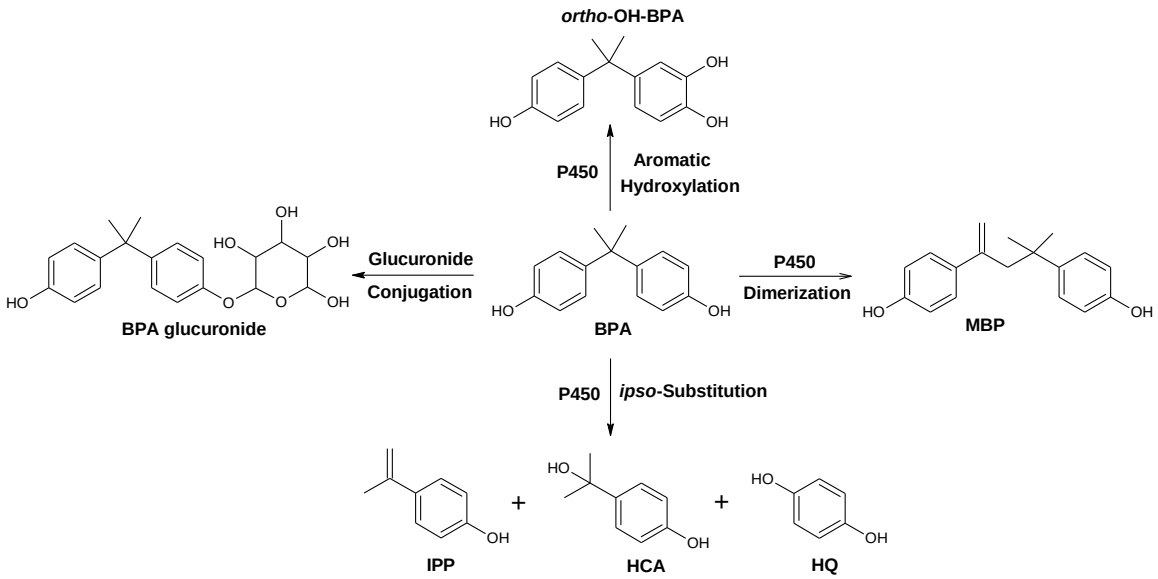

Formation of metabolites via *ipso*-substitution constitutes about 20% of the competing *ortho*-OH-BPA formation via traditional aromatic hydroxylation by P450,[13] i.e. *ipso*-substitution is quantitatively important in competition with the traditional aromatic hydroxylation of phenolic EDCs. Oxidation of diverse *p*-substituted phenols by rat liver P450 has been found to result in elimination of the substituents, including -NO_2, -CH_2OH, -$COCH_3$, -COPh, -COOH, -F, -Cl, and –Br.[21] Accordingly, *ipso*-substitution can be categorized into two types depending on the group eliminated from the quinol intermediate.[21,22] As shown in **Scheme 2**, type I *ipso*-substitution implies that the substituent eliminates as an anion with formation of a quinone, whereas in type II *ipso*-substitution the eliminating group is a cation, leading to the formation of a hydroquinone.[21] However, during oxidation of 4-n-nonylphenol, estrone, estradiol etc. by P450, *ipso*-addition quinol was formed without C-C bond cleavage.[23,24] Therefore, the *ipso*-substitution, *ipso*-addition, as well as the above-mentioned aromatic hydroxylation mechanisms compete under various conditions as relevant pathways, and understanding these mechanisms at the molecular level seems necessary to access the environmental toxicity and fate of phenolic EDCs. However, the active species of P450, the iron(IV)-oxo heme cation radical Compound I (Cpd I), responsible for P450-catalyzed oxidations in all P450 isoenzymes, is short-lived and one of the most potent oxidants in nature,[25,26] and thus several details of its catalytic action are inaccessible by standard experimental methods. Specially, two possible pathways for P450-catalyzed *ipso*-substitution via a quinol intermediate should be distinguished; one involveing initial formation of a phenoxy radical and the other involving the formation of an epoxide via O-addition.[27-29]

Analysis of enzyme mechanisms using computational chemistry may identify with semi-quantitative accuracy the electronic structure features governing reactivity.[30-38] Density functional theory (DFT) has been used to study many P450-catalyzed oxygenation reactions including

hydroxylation of C-H bonds, epoxidation of C=C bonds, oxidation of aromatic rings, oxidation of heteroatoms etc.[33] The main goal of this work is to show how DFT can be used to elucidate the full molecular mechanism of the P450-dependent metabolism of phenolic EDCs and to identify how and when environmentally related *ipso*-substitution, and formation of the very estrogenic dimer-type metabolites can occur. BPA was used to obtain the full mechanistic picture because of its prominence in the environment,[39,40] with rich experimental data of its P450-catalyzed metabolism[13,14] for validation of the computationally obtained mechanisms. The work was extended to also study the P450-catalyzed biotransformation mechanisms of several other widely-used phenolic EDCs, such as bisphenol analogues, alkylphenols and chlorophenols. The fundamental electronic drivers that govern *ipso*-addition vs. *ipso*-substitution and type I vs. type II substitute elimination were identified, directly relevant for screening P450-catalyzed biotransformation of many emerging environmental phenolic EDCs.

Scheme 2. Proposed *ipso*-Substitution Mechanisms of P450-Catalyzed Substituent Elimination[a]

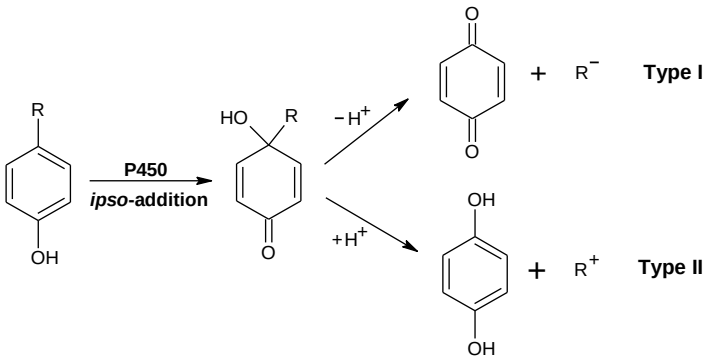

[a] The reactive position is defined as the *ipso*-position; R represents the elimination substituent.

Computational Methodology

DFT Calculations with Cpd I of P450. As is common practice,[29,41-43] the six-coordinate tri-radicaloid ferryl complex $Fe^{4+}O^{2-}(C_{20}N_4H_{12})^{-1}(SH)^{-1}$ was used to model the enzymatic active site of Cpd I of P450. Cpd I of P450 exists in two close-lying electronic states, a high-spin (HS) quartet state and a low-spin (LS) doublet state.[33,44] All geometries on both the LS and HS routes were optimized with unrestricted DFT using the B3LYP hybrid density functional[45,46] in combination with the LAN2DZ basis set[47] on iron and 6–31G on other atoms (denoted BSI). B3LYP was chosen because it can reproduce measured kinetic isotope effects for P450-catalyzed reactions,[48] electron paramagnetic resonance parameters for penta-coordinated heme in P450 enzyme,[49] generate geometries consistent with crystal structures,[50] and show qualitatively accurate relative energies vs. benchmark CASSCF calculations.[51] Intrinsic reaction coordinate (IRC) calculations were performed to verify the rate-determining transition states connecting the reactants and intermediates on the potential energy surface (**Figure S1-S22** in the Supporting Information). Please note that the basis-set superposition error (BSSE) has been reported to be very small for reactant complexes of P450-catalyzed oxidation reactions,[52] but they may affect the relative energies of very large vs. small substrates and thus we did not include these minor contributions to the energies in the following as our substrates are similar in size and type.

In order to evaluate broadly the sensitivity of the reaction mechanism toward the choice of density functional, in addition to the B3LYP energies (**Table S1** in the Supporting Information), we performed unrestricted single-point calculations with other hybrid, local, and non-hybrid functionals, i.e. TPSSh,[53,54] B3PW91,[46,55] BLYP[45,56] MPW1PW91,[57] and M06L[58] using the B3LYP/BSI optimized geometries for the P450-catalyzed metabolic mechanisms of BPA (**Table S2** in the Supporting Information). The same qualitative picture was obtained with all of the

functionals, and we therefore focused in the following on the B3LYP results. To test the basis set effect on geometry optimization, the molecular species involved in the initial H-abstraction from the phenolic group as well as in the O-addition to the aromatic ring of BPA were optimized at the B3LYP/BSI** level, producing few geometrical and energetic discrepancies as compared with the results obtained at the B3LYP/BSI level (detailed data in **Table S3** and **Figure S23** in the Supporting Information). Hence the basis set BSI was used for geometry optimizations throughout the remaining work.

Analytical frequency calculations were used to ensure that there was no imaginary frequency for any ground state, and only one imaginary frequency for all transition states. The vibrational frequencies were also used to calculate the zero-point energy (ZPE) and thermal and entropic corrections to the free energy at 298.15 K and 101.325 kPa. More accurate energies were obtained using single-point calculations with the SDD[59] basis set on iron and the 6–311++G** basis set for all other atoms (denoted BSII). Bulk polarity effects were evaluated by the PCM solvation model[60] using chlorobenzene with a dielectric constant of 5.6 at the B3LYP/BSI level; this dielectric constant provides a good estimate of the polarization caused by the dipoles of the protein pocket near the axial cysteine.[61] We also evaluated the bulk polarity effect using the SMD solvation model[62] for the P450-catalyzed mechanisms of BPA; the H-abstraction and O-addition steps occurred with only slightly higher energies (**Table S4** in the Supporting Information). In addition, we evaluated PCM energies using cyclohexane (ε=2.0), 1-bromopropane (ε=8.0), ethanol (ε=24.9), and acetonitrile (ε=35.7). Except for a minor difference in energy for the oxidation of BPA, the same qualitative picture was obtained throughout (**Table S5** in the Supporting Information). Dispersion interactions were considered by performing single-point energy calculations with the B3LYP-D3/BSI level since B3LYP itself does not include dispersion by design.[63] The relative free

energies of the P450 oxidation reactions shown below were estimated by combining B3LYP/BSII single-point energies with PCM solvation and dispersion corrections, as well as Gibbs free energy corrections from optimizations at the BSI level, unless pointed out specifically.

The cluster approach of studying the reaction mechanism treats the catalytic active site of the enzyme by including key surrounding amino acids and treating all these interactions fully quantum mechanically.[38] BPA is mainly catalyzed by P450 isoforms 3A4 and 3A5,[13] and therefore we used the P450 3A4 crystal structure (PDB code: 1W0G)[64] to produce a larger model of the active site. As shown in **Figure S24** in the Supporting Information, the Cpd I model is the same in the large and small model, whereas six important second-shell residues, ARG105, ILE301, THR309 and ALA370 and the peptide chain of ALA305−GLY306 have been included in the large model, with key central atoms locked in their crystallographic positions to maintain the protein scaffold packing, steric effects, and hydrogen bond geometries. The large model is charge-neutral and contains 138 atoms, and the reaction mechanism was investigated for both the HS and LS states. The geometry optimization, more accurate single-point calculations, evaluation of the bulk polarity effects, and dispersion interactions were all performed in the same way for both the large and small models. The results are discussed in detail in the Supporting Information, where all energies are compiled in **Tables S1-S31**. Importantly, we conclude that the small and large models are in good agreement on the preferred pathways (**Figure S25** in the Supporting Information), probably because the main energy effects and electronic reorganizations occur near the iron-oxygen moiety. We thus performed an extended series of calculations based on the small model as discussed below.

Reaction Energy Calculations for the Decomposition of Quinol Intermediates. All geometries for the decomposition reactions of various *ipso*-addition quinol intermediates from P450-catalyzed *ipso*-position metabolism were optimized at the B3LYP/6-31G** level in water

solution (ε=78.4) with PCM. Then based on the optimized structures, single-point calculations were performed in PCM water solution with D3 dispersion corrections at the B3LYP/6-311++G** level. The reported reaction free energies for decomposition of quinol intermediates are described by PCM//B3LYP/6-311++G** with water solution and D3 dispersion corrections, as well as free energy corrections from B3LYP/6-31G** geometry optimizations.

All calculations of this work were carried out with the Gaussian 09 D.01 program package.[65]

Results and Discussion

Reaction Mechanisms of P450-Catalyzed Bisphenol A

H-abstraction vs. O-addition. Figure 1 shows two computed competitive reaction mechanisms of BPA catalyzed by P450, one involving initial H-abstraction from the phenolic group, and the other involving initial O-addition to the π-system of the aromatic ring. As is common in P450 reactions,[33] both the HS and LS pathways are available due to the near-degenerate states of Cpd I. The reactions start from reactant complexes (^{4,2}RC), in which the H-atom of the phenolic group of BPA interacts with the iron-oxo moiety of Cpd I. Then, ^{4,2}RC may go through H-abstraction transition states $^{4,2}TS_H$ with formation of the intermediate complexes ($^{4,2}I_H$) involving iron-hydroxo species and the phenoxy radical of BPA. The HS transition state $^{4}TS_H$ appears slightly later on the reaction coordinate than its LS counterpart $^{2}TS_H$, with BPA−O···H and H···O−Fe distances of 1.211 vs. 1.207 Å and 1.203 vs. 1.212 Å, respectively. These H-abstraction transition states are characterized by almost linear O···H···O configurations as well as large imaginary frequencies (HS: *i*1521 cm^{-1}; LS: *i*1569 cm^{-1}). Cpd I is a potent H-atom abstractor toward the phenolic group, with a H-abstraction barrier of only 0.4/0.3 kcal/mol for the HS/LS state, similar to the minor H-abstraction barriers obtained for the phenolic group of paracetamol[29]

and the amino group of anilines[42], yet much lower than the H-abstraction barriers obtained from C−H hydroxylation.[41,52,66] In addition, the formed complex intermediates ($^{4,2}I_H$) are stable, with exothermic reaction energies of -8.0/-7.4 kcal/mol for the HS/LS state. Note that dispersion effects lower the H-abstraction barriers by a substantial 2.5 kcal/mol, a magnitude consistent with previous findings for P450 reactions.[67]

Another possible reaction path starting from ^{4,2}RC is the addition of the oxo group of Cpd I onto the unsubstituted aromatic ring of BPA via C-O bond-forming transition states $^{4,2}TS_O$, which produce tetrahedral intermediates. As shown in **Figure 1**, compared with the LS species, TS_O in the HS state is more advanced (shorter O···C bond) with a higher degree of aromatic activation. The calculated barriers for O-addition at the *ortho*-position ($^{4,2}TS_{Oo}$) and *meta*-position ($^{4,2}TS_{Om}$) are 17.5/14.5 and 19.9/17.1 kcal/mol, respectively, on the HS/LS state surfaces. Comparison of the barriers of the H-abstraction and O-addition steps shows clearly that the H-abstraction reaction is much more favorable. Therefore, we focused on the H-abstraction pathway in the following sections.

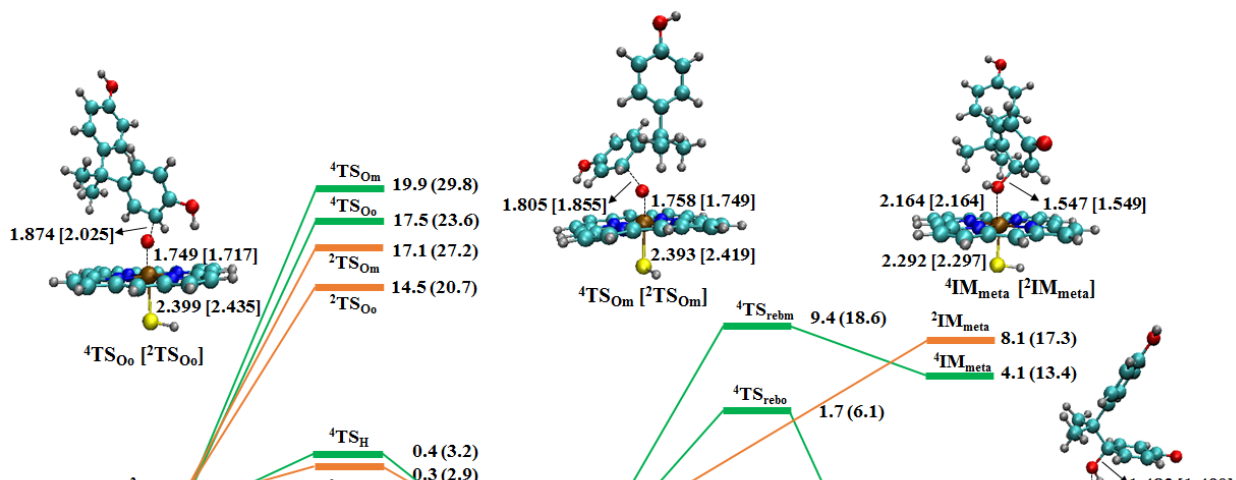

Figure 1. Free energy profile of BPA catalyzed by Cpd I of P450, along with the optimized geometries of the key reaction species in the HS and LS states. Free energies (kcal/mol) are relative to the quartet reactant complex ^{4}RC at the B3LYP/BSII//BSI level including solvation (ε=5.6) and dispersion corrections (no parentheses), and without dispersion (in parentheses). Geometrical parameters (lengths in Å and angles in degrees) are shown as the HS [LS] state.

OH Radical Rebound Mechanism. For the H-abstraction pathway, formation of the intermediate complex (^{4,2}IM$_{H}$) is followed by rebound of the phenoxy radical onto the iron-hydroxo species. This occurs via formation of covalent bonds at the *ipso*-, *ortho*- or *meta*-carbon of the aromatic ring of BPA to yield corresponding addition quinol intermediates IM$_{ipso}$, IM$_{ortho}$ or IM$_{meta}$. As shown in **Figure 1**, all the rebound steps are essentially barrierless in the LS state, while they proceed with significant barriers of 7.8-17.4 kcal/mol on the HS surface. The rebound reactions at the *ipso*- and *ortho*-carbon are exothermic for both the HS and LS pathways, with reaction energies of -31.6/-29.5 and -30.3/-32.7 kcal/mol, respectively, while the rebound reactions

at the *meta*-carbon are endothermic (+4.1/+8.1 kcal/mol). Importantly, the thermodynamically unfavorable rebound reactions associated with this mechanism can explain the lack of experimental detection of the hydroxylation product of the *meta*-position during P450-dependent metabolism of BPA.[13] Note that the HS rebound barriers are significantly larger than the initial H-abstraction barriers, implying that ^{4}Cpd I is a sluggish oxidant and unlikely to play a key role. Thus, OH recombination with the phenyl ring of BPA only occurs via the LS potential energy surface. Accordingly, OH radical rebound will proceed under thermodynamic control, and the reaction energy difference between formation of IM_{ortho} of -32.7 kcal/mol and IM_{ipso} of -29.5 kcal/mol for the LS state of about 3.2 kcal/mol, favors IM_{ortho} formation but also translates into a lower fraction of IM_{ipso} formed. This is in accordance with the observation that metabolites formed via *ipso*-substitution constitute approximately 20% of the products of the traditional aromatic hydroxylation pathway of P450.[13]

Decomposition Reaction of the Quinol Intermediate (IM_{ipso}) of BPA. Hydroquinone, isopropenylphenol (IPP), and hydroxycumyl alcohol (HCA) were detected as metabolites upon C-C bond scission via *ipso*-substitution in experiments of the P450-catalyzed degradation of BPA,[13,68] which means that the *ipso*-metabolism reaction of BPA does not stop in the quinol form. In order to understand the complete mechanistic picture, we need to establish the nature of the quinol intermediate decomposition. As mentioned above, there are two types of substituent elimination from the quinol intermediate. While hydroquinone has been detected in the experiments of oxidation of BPA by P450,[13,68-70] quinone is also easily transformed to hydroquinone upon NADPH-induced reduction in rat liver microsomes.[21] Therefore, it is difficult to conclude whether the decomposition of the *ipso*-addition quinol intermediate (IM_{ipso}) proceeds via type I or type II elimination based on the available experimental data.

Table 1. Computed Aqueous-Phase Free Energies (ΔG) (kcal/mol) for the Decomposition Reactions of Quinol of BPA

Condition	Elimination Type	ΔG (kcal/mol)
Neutralization	**Type I** 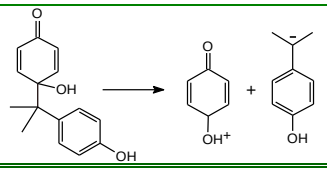	**82.1**
Neutralization	**Type II** 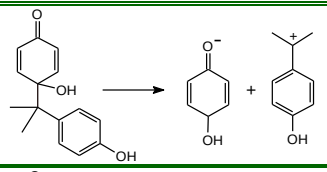	**11.1**
Deprotonation	**Type I** 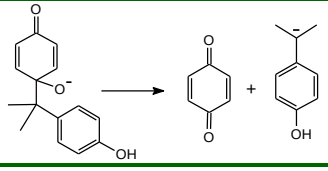	**21.8**
Protonation	**Type II** 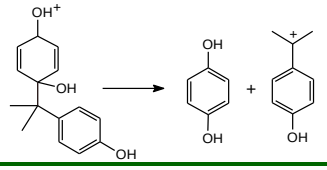	**-30.7**

As shown in **Table 1**, the heterolytic decomposition of IM_{ipso} may proceed charge-neutrally or after protonation or deprotonation in water solution. The computations suggest that the charge-neutral decompositions of IM_{ipso} leading to a carbocation (type II *ipso*-substitution) or carbanion intermediate (type I *ipso*-substitution) have reaction energies of +11.1 kcal/mol and +82.1 kcal/mol, respectively. The decomposition of IM_{ipso} after deprotonation (type I *ipso*-substitution) is endothermic by +21.8 kcal/mol. Thus, the most feasible pathway is decomposition after protonation with production of the carbocationic intermediate and hydroquinone (type II *ipso*-substitution) with a reaction energy of -30.7 kcal/mol, which supports that the quinol intermediate generated in the P450 enzyme pocket can readily dissociate from the pocket and decompose in a nonenzymatic environment after protonation.

The carbocationic intermediate can react to produce IPP by fast proton transfer to a hydroxyl ion with a reaction energy of -48.7 kcal/mol, or into HCA by absorbing the hydroxyl ion with a reaction energy of -44.0 kcal/mol (using the same method of calculations as for the decomposition of quinols). This mechanism would explain the puzzling observation that no quinol of BPA has ever been detected as an *ipso*-addition metabolite:[13,68-70] From our reaction diagrams, it is an unstable intermediate that quickly collapses to the product.

MBP Formation. A dimer-type metabolite MBP has been shown to exhibit the highest estrogen activity among all BPA metabolites, and thus we investigated also the MBP formation mechanism. First, we examined the feasibility of the previously suggested radical pathway of MBP formation; this reaction occurs between the isopropenylphenol radical formed by oxidative cleavage of the carbon–phenyl bond, and IPP, as supported by the disappearance of the mass peak of MBP when a radical scavenger was added to the incubation system.[14] However, as shown in **Table S31** in the Supporting Information, the cleavage reactions of the carbon–phenyl bond of BPA and the phenoxy radical of BPA in the enzymatic environment are both highly endothermic, and thus the radical pathway seems unfavorable. According to LC/MS/MS investigation, the metabolite of BPA gave a negative mass peak at $[M–H]^-$ 267 in LC/MS and a single daughter ion at m/z 133 on MS/MS analysis, corresponding to MBP and IPP, respectively.[14] Alternatively, the dimer-type structure of MBP triggers cationic polymerization, by which the carbocation reacts with IPP, with both reactants originating from the *ipso*-substitution pathway, initiating polymerization and generation of MBP, as shown in eq 1:

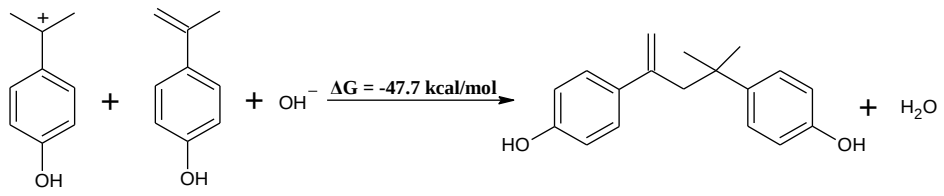

(1)

The obtained reaction energy of −47.7 kcal/mol provides a notable driving force for this cationic polymerization pathway to form MBP (using the same method of calculation as for the decomposition of quinols). The P450-catalyzed *ipso*-substitution suggested above proceeds through the radical pathway involving H-abstraction from BPA to produce a phenoxy radical, which would explain why adding a radical scavenger to the incubation system prevents MBP formation during the experiment.

The Reaction Patterns of P450-Catalyzed *ipso*-Position Metabolism

Initial Rate-Determining Step for the Production of *ipso*-Addition Quinol Intermediates. In order to study the detailed reaction mechanism and to verify the initial rate-determining step for *ipso*-position metabolism, we studied several other widely-used phenolic EDCs distributed in the environment such as bisphenol analogues, alkylphenols and chlorophenols with available *in vitro* or *in vivo* assay data on the P450 metabolism.[3,14,15,21,23,71] As shown in **Table 2**, these phenolic EDCs include bisphenol F (BPF), bisphenol B (BPB), tetrabromobisphenol A (TBBPA), dimethylbisphenol A (DMBPA), bisphenol AF (BPAF), bisphenol Z (BPZ), 4-n-nonylphenol (NP1), *p*-hydroxybenzoic acid (PHBA), *p*-cresol (PC), and *p*-chlorophenol (PCP). The relative energies of the H-abstraction from the phenolic group as well as O-addition at the aromatic *ortho*-carbon position on the LS potential energy surface are listed in **Table 2**. The barriers of H-abstraction (0.4-3.1 kcal/mol) are much lower than that for O-addition (14.2-21.0 kcal/mol) for all phenolic EDCs, i.e. the initial step involves H-abstraction by Cpd I from the phenolic group leading to an intermediate complex consisting of an iron-hydroxo group and a phenoxy radical. Within the intermediate complex, as in the reaction of BPA catalyzed by P450, the OH rebounds onto both the *ipso*- and *ortho*-carbon to form the hydroxylation intermediates with markedly

exothermic reaction energies (-36.3 to -16.5 kcal/mol). The OH rebound barriers for the HS pathway (4.4-13.5 kcal/mol) are much higher than the initial H-abstraction barriers (see details in **Table S9** in the Supporting Information), while the OH rebound on the LS pathway is essentially barrier-free. Therefore, we suggest that the P450-catalyzed *ipso*-position metabolism of these diverse phenolic EDCs follows the same reaction mode as displayed in **Figure 1** of BPA, i.e. via H-abstraction followed by an essentially barrierless OH rebound onto the *ipso*-carbon to produce the corresponding *ipso*-addition quinol intermediate mainly via the LS state.

As shown in **Table 2**, compared with the thermodynamic data on OH rebound onto the *ortho*-positions, the rebound reactions onto the *ipso*-positions are 2.3 and 2.6 kcal/mol more favorable for PCP and NP1, respectively, but 0.7-9.1 kcal/mol less favorable for all other phenolic EDCs. Although the driving force for *ortho*-addition relative to *ipso*-addition is much larger for PBHA, BPAF and TBBPA, the obtained energy difference of 6-9 kcal/mol may still translate into a lower fraction of the *ipso*-addition quinol intermediates. Regardless of the external factors, we conclude that the P450-catalyzed *ipso*-position metabolism competes with *ortho*-position metabolism in the LS state under thermodynamic control. This is consistent with the experiments, in which *ipso*-substitution/addition metabolites of all studied phenolic EDCs studied in this work were observed in the presence of P450, such as 4-hexafluorohydroxyisopropilidene-phenol from BPAF, and 2,6-dibromo-4-(2-hydroxypropane-2-yl) phenol from TBBPA, which may be produced by the addition of hydroxyl ion to the carbocations as the *ipso*-substitution products, as well as 4-nonyl-4-hydroxy-cyclohexa-2,5-dienone produced from 4-NP1 as the *ipso*-addition product. Until now, there are no reported ratios of *ipso*-addition vs. *ortho*-addition products for most phenolic EDCs. However, the calculated energy difference between *ipso*-addition and *ortho*-addition can be used as a probe for predicting the relative importance of these two pathways.

Table 2. Relative Free Energies (kcal/mol) for P450-catalyzed *ipso*-Position Metabolism of Phenolic EDCs via the LS state

Phenolic EDCs			^2TS_H	$^2TS_{Oo}$	^2IM_H	$^2IM_{ipso}$	$^2IM_{ortho}$	ΔG_{gap}
Bisphenol Analogues	BPF	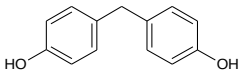	2.1	16.6	-6.6	-32.3	-33.0	0.7
	BPB	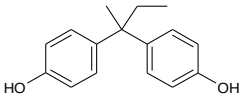	1.2	14.2	-6.5	-30.5	-34.1	3.6
	TBBPA	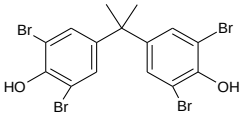	0.4	19.9	-6.7	-30.1	-36.3	6.2
	DMBPA	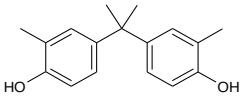	0.4	15.4	-7.8	-30.3	-33.7	3.4
	BPAF	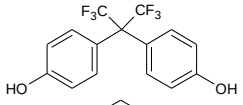	3.1	19.5	0.6	-17.0	-26.1	9.1
	BPZ	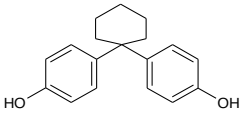	1.8	16.1	-6.0	-29.0	-32.3	3.3
Alkylphenols	NP1	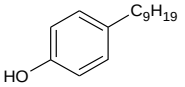	1.6	18.2	-5.9	-32.4	-29.8	-2.6
	PHBA	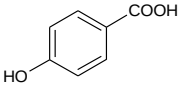	3.0	21.0	1.6	-16.5	-23.6	7.1
	PC	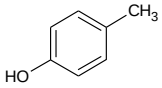	2.7	17.8	-6.8	-28.8	-30.6	1.8
Chlorophenols	PCP	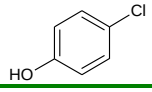	2.8	20.1	-2.9	-29.0	-26.7	-2.3

Decomposition Reaction Mechanisms of Diverse Quinol Intermediates. Experimental work on P450-catalyzed phenolic EDCs has shown that *ipso*-substitution prior to *ipso*-addition does not always occur.[21,23,24,69] However, the reason why some phenolic EDCs are stopped at the *ipso*-addition step is unknown. It is also difficult to determine which type of elimination (type I or type II) occurs during *ipso*-substitution due to the complex biological redox environment. We focused on the decomposition mechanisms of the diverse *ipso*-addition quinol intermediates

derived from the diverse phenolic EDCs described above with the available experimental information,[21,69] but excluded TBBPA and BPZ, for which our attempts to locate the quinol intermediates after protonation give fragmental type II products directly. The thermodynamic data for the decomposition of quinol intermediates in all possible pathways were evaluated and the most favorable decomposition paths via type II and type I *ipso*-substitution are shown in **Figure 2**.

Figure 2. Computed free energies (kcal/mol) for the decomposition reactions of diverse *ipso*-addition quinols along the favorable pathways: (left) type II substitution with the hydride ion affinity (HIA, kcal/mol) of the formed carbocation; (right) type I substitution. [a] R represents the elimination substituent.

As shown in **Figure 2**, for all bisphenol analogues and alkylphenols except for PHBA, the decomposition of the formed *ipso*-addition quinols after protonation with formation of carbocation and hydroquinone (type II substitution) is the most favorable pathway. The decomposition

reactions for the *ipso*-addition quinols from PC and NP1 are distinctly endothermic, which is fully in line with experimental observations of the P450-catalyzed conversion of these two alkylphenols showing only *ipso*-addition quinols were produced without detecting any *ipso*-substitution products.[21,23,69] However, for other bisphenol analogues and alkylphenols, the decomposition of the formed *ipso*-addition quinols after protonation can proceed, leading to C-C bond cleavage with significant exothermic energies. It is found that the P450-catalyzed *ipso*-substitution products are obtained from the *ipso*-addition quinols when the carbon at the benzylic position contains one or more alkyl branches. More alkyl branches stabilize the carbocation via inductive and hyperconjugative effects; this results in the spontaneous decomposition of the formed *ipso*-addition quinols after protonation. The hydride ion affinity (HIA) can be used for comparing the carbocation stability of dissimilar structures directly, defined according to eq (2):[72]

$$RH \longrightarrow R^+ + H^- \quad \Delta H^0 = HIA \tag{2}$$

The HIA obtained at the B3LYP/6-311++G** level using frequency analysis at 298.15 K and 1 atm pressure are listed in the lower left of **Figure 2**. The experimental HIA is available for CH_3^+ (312 kcal/mol),[72] the same as the computed HIA of 312 kcal/mol, which supports the reliability of the computational method. The reaction free energies of decomposition of the quinol intermediates generally increase with increasing HIA of the formed carbocations (r^2 = 0.95, $\Delta G = 1.4HIA + 245.5$). This pattern indicates that the HIA values are useful for preliminary evaluation of the decomposition free energies of the *ipso*-addition quinols produced from bisphenol analogues and alkylphenols with associated formation of a carbocation and a hydroquinone (type II substitution).

For quinol intermediates with electronegative substituents, such as -Cl and -COOH, as shown in **Figure 2**, there are two possible pathways for substituent elimination from quinol with the formation of an anion and a quinone (type I *ipso*-substitution): 1) elimination of the substituent

after deprotonation with the formation of an anion and quinone; 2) involving the prior intra-molecular H-arrangement from OH to the electronegative substituents to produce the corresponding inorganic acid and quinone neutrally. The charge-neutral intra-molecular H-arrangement pathway with formation of the inorganic acid and quinone is more favorable for decomposition of quinol intermediates with electronegative substituents; in this case the inorganic acid can dissociate into an anion. The pathway we have obtained for type I *ipso*-substitution extends the formal definition of type I *ipso*-substitution in P450 chemistry. In particular, the elimination of -COOH from quinol after deprotonation is not feasible because it is endothermic, while the exothermic elimination of -COOH during the intra-molecular H-arrangement route is favorable. This is in accordance with the experimental observation that PHBA can be subject to *ipso*-substitution when the reaction is catalyzed by P450.[21]

Environmental Implications

Identification of EDCs is one of the most important goals of environmental chemical hazard screening, which has come a long way in developing useful test assays and mechanism-based screening techniques.[10] Many synthetic compounds released into the environment may be readily transformed, especially by P450 enzymes, into metabolites exhibiting much higher endocrine-disrupting activity than their parent compounds. Knowledge of detailed metabolic mechanisms gives insight into the bioactivation. Accordingly, it is critical in environmental risk assessment to understand metabolic pathways and to have effective tools for predicting the fate of metabolites. Methods that analyze and predict the metabolic fate of molecules thrive within the field of medicinal chemistry,[73] but not so much within environmental sciences despite the similarity of involved tools. In medicinal chemistry, many drugs require P450-mediated bioactivation to elicit their pharmacological effect via metabolites that can be characterized in relatively high

concentrations. In contrast, environmental pollutants such as EDCs and their metabolites normally occur in trace amounts while still important at these levels, and thus identification of their biotransformation products seems more difficult, and mechanism-based methods to provide putative metabolites efficiently are of interest. Experimental methods often require expensive equipment, expertise, running costs and time, which may reduce their applicability when screening large libraries of compounds. Thus, there is substantial interest in the development of fast, accurate computational tools that can predict metabolism with higher throughput and lower cost. These computational tools should: (i) predict the site of metabolism and (ii) predict the metabolite structure from these sites.[74]

The present work shows how detailed DFT investigations of metabolic pathways can rationalize the formation of metabolites resulting from the P450-catalyzed reactions of diverse environmental phenolic EDCs such as bisphenol analogues, alkylphenols and chlorophenols, thereby achieving these two tasks, as particularly emphasized for one of the prominent phenolic EDCs, BPA. The barrier for the most favorable H-abstraction/OH-rebound mechanism involving both the *ipso*- and *ortho*-position hydroxylation is one of the lowest reported barriers, as far as we know. The H-abstraction/OH-rebound reaction with formation of the quinol intermediate seems to be a general reaction mechanism for phenolic EDCs, as shown by studying a diverse group of such compounds in this work. In case of the *ipso*-addition quinol intermediate, we can distinguish type II vs. type I *ipso*-substitutions based on thermodynamic data, and *ipso*-substitution vs. *ipso*-addition based on the stability of the eliminating carbocation by both qualitative and quantitative analysis. Notably, the formation mechanism of the highly estrogenic metabolites HCA and dimer-type MBP, which arises from oxidation of BPA catalyzed by P450, has been revealed in detail. Our results show that both metabolites originate from a carbocationic intermediate produced in the

ipso-substitution pathway. This pathway gives insight into the potentially important bioactivation of many other alternatives to BPA whose metabolic mechanisms remain unidentified, in particular under conditions where P450-catalyzed metabolism is important relative to glucuronidation (e.g. if this pathway is inhibited or genetically or otherwise down-regulated, e.g. in the fetus). However, even when non-P450 pathways dominates by 10-, 100- or even 1000-fold, the *ipso*-position metabolites may still contribute to toxicity due to their correspondingly higher potency.

The hydroxylated metabolites of many emerging phenolic pollutants, such as OH-PBDEs and OH-PCBs, have been reported to be even stronger EDCs than their precursors,[75,76] and based on their similar molecular structures we speculate that they may involve products from the *ipso*-substitution/addition pathway catalyzed by P450, which has thus far largely been neglected. Recently, the biotransformation of sulfonamide antibiotics in the environment has been reported to proceed via the *ipso*-substitution pathway.[77] Therefore, *ipso*-substitution seems to be a much more common and, even at low turnover, more important toxification pathway than previously thought for a wide variety of persistent pollutants. Our study has identified the detailed electronic structure changes and transition states probably involved in these processes, as well as provided simple tools for determining the relative importance of these pathways based on thermodynamic considerations that we envision will be valuable for determining the environmental toxicity and fate of emerging phenolic EDCs.

ASSOCIATED CONTENT

Supporting Information. Full citation for reference 73; Energies for all molecular species; Intrinsic reaction coordinate (IRC) for verifying transition states; Optimized geometries at the

B3LYP/BSI** level of theory; Quantum chemical cluster calculations; Cartesian coordinates of all structures. This material is available free of charge via the Internet at http://pubs.acs.org.

Corresponding Author

*(L.J.) E-mail: jilienv@zju.edu.cn

*(K.P.K.) E-mail: kpj@kemi.dtu.dk

Notes

The authors declare no competing financial interest.

ACKNOWLEDGMENT

This work was supported by the National Natural Science Foundation of China (21677125). The China National Supercomputing Center in Shenzhen and UFZ in Leipzig are acknowledged for providing the Gaussian 09 package and the high-performance computing clusters. We also thank the general agreement on cooperation between UFZ Germany and Zhejiang University China (No. RA-127/13) to give Dr. Li Ji a guest scientist status in UFZ between 2013 and 2015 to have access to the computing clusters of UFZ.

REFERENCES

(1) Gaines, T. B.; Hayes, W. J.; Linder, R. E. Liver metabolism of anticholinesterase compounds in live rats: Relation to toxicity. *Nature* **1966,** *209*, (5018), 88-89.

(2) Ashrap, P.; Zheng, G. M.; Wan, Y.; Li, T.; Hu, W. X.; Li, W. J.; Zhang, H.; Zhang, Z. B.; Hu, J. Y. Discovery of a widespread metabolic pathway within and among phenolic xenobiotics. *Proc. Natl. Acad. Sci. U. S. A.* **2017,** *114*, (23), 6062-6067.

(3) Chen, D.; Kannan, K.; Tan, H.; Zheng, Z.; Feng, Y. L.; Wu, Y.; Widelka, M. Bisphenol analogues other than BPA: environmental occurrence, human exposure, and toxicity-a review. *Environ. Sci. Technol.* **2016,** *50*, (11), 5438-5453.

(4) Reinen, J.; Vermeulen, N. P. Biotransformation of endocrine disrupting compounds by selected phase I and phase II enzymes--formation of estrogenic and chemically reactive metabolites by cytochromes P450 and sulfotransferases. *Curr. Med. Chem.* **2015,** *22*, (4), 500-527.

(5) Guengerich, F. P. Common and uncommon cytochrome P450 reactions related to metabolism and chemical toxicity. *Chem. Res. Toxicol.* **2001,** *14*, (6), 611-650.

(6) Guengerich, F. P. Cytochrome P450 and chemical toxicology. *Chem. Res. Toxicol.* **2008,** *21*, (1), 70-83.

(7) Ribalta, C.; Sole, M. *In vitro* interaction of emerging contaminants with the cytochrome P450 system of Mediterranean deep-sea fish. *Environ. Sci. Technol.* **2014,** *48*, (20), 12327-12335.

(8) Yoo, J.; Hirano, M.; Mizukawa, H.; Nomiyama, K.; Agusa, T.; Kim, E. Y.; Tanabe, S.; Iwata, H. *In vitro* and *in silico* analyses for predicting hepatic cytochrome P450-dependent metabolic potencies of polychlorinated biphenyls in the Baikal seal. *Environ. Sci. Technol.* **2015,** *49*, (24), 14588-14596.

(9) Fu, Z. Q.; Wang, Y.; Chen, J. W.; Wang, Z. Y.; Wang, X. B. How PBDEs are transformed into dihydroxylated and dioxin metabolites catalyzed by the active center of cytochrome P450s: a DFT study. *Environ. Sci. Technol.* **2016,** *50*, (15), 8155-8163.

(10) Khetan, S. K. *Endocrine Disruptors in the Environment*. John Wiley & Sons, Inc.: Hoboken, New Jersey, 2014.

(11) Welshons, W. V.; Nagel, S. C.; vom Saal, F. S. Large effects from small exposures. III. Endocrine mechanisms mediating effects of bisphenol A at levels of human exposure. *Endocrinology* **2006,** *147*, (6 Suppl), S56-69.

(12) Quesnot, N.; Bucher, S.; Fromenty, B.; Robin, M. A. Modulation of metabolizing enzymes by bisphenol a in human and animal models. *Chem. Res. Toxicol.* **2014,** *27*, (9), 1463-1473.

(13) Nakamura, S.; Tezuka, Y.; Ushiyama, A.; Kawashima, C.; Kitagawara, Y.; Takahashi, K.; Ohta, S.; Mashino, T. *Ipso* substitution of bisphenol A catalyzed by microsomal cytochrome P450 and enhancement of estrogenic activity. *Toxicol. Lett.* **2011,** *203*, (1), 92-95.

(14) Yoshihara, S.; Mizutare, T.; Makishima, M.; Suzuki, N.; Fujimoto, N.; Igarashi, K.; Ohta, S. Potent estrogenic metabolites of bisphenol A and bisphenol B formed by rat liver S9 fraction: their structures and estrogenic potency. *Toxicol. Sci.* **2004,** *78*, (1), 50-59.

(15) Gramec Skledar, D.; Peterlin Masic, L. Bisphenol A and its analogs: Do their metabolites have endocrine activity? *Environ. Toxicol. Pharmacol.* **2016,** *47*, 182-199.

(16) Pacifici, G. M.; Kubrich, M.; Giuliani, L.; de Vries, M.; Rane, A. Sulphation and glucuronidation of ritodrine in human foetal and adult tissues. *Eur. J. Clin. Pharmacol.* **1993,** *44*, (3), 259-264.

559 (17) Hakkola, J.; Pelkonen, O.; Pasanen, M.; Raunio, H. Xenobiotic-metabolizing cytochrome
560 P450 enzymes in the human feto-placental unit: role in intrauterine toxicity. *Crit. Rev. Toxicol.*
561 **1998,** *28*, (1), 35-72.

562 (18) Hakkola, J.; Raunio, H.; Purkunen, R.; Saarikoski, S.; Vahakangas, K.; Pelkonen, O.;
563 Edwards, R. J.; Boobis, A. R.; Pasanen, M. Cytochrome P450 3A expression in the human fetal
564 liver: evidence that CYP3A5 is expressed in only a limited number of fetal livers. *Biol. Neonate*
565 **2001,** *80*, (3), 193-201.

566 (19) Nahar, M. S.; Liao, C.; Kannan, K.; Dolinoy, D. C. Fetal liver bisphenol A concentrations
567 and biotransformation gene expression reveal variable exposure and altered capacity for
568 metabolism in humans. *J. Biochem. Mol. Toxicol.* **2013,** *27*, (2), 116-123.

569 (20) Nahar, M. S.; Liao, C.; Kannan, K.; Harris, C.; Dolinoy, D. C. In utero bisphenol A
570 concentration, metabolism, and global DNA methylation across matched placenta, kidney, and
571 liver in the human fetus. *Chemosphere* **2015,** *124*, 54-60.

572 (21) Ohe, T.; Mashino, T.; Hirobe, M. Substituent elimination from *p*-substituted phenols by
573 cytochrome P450. *ipso*-Substitution by the oxygen atom of the active species. *Drug Metab. Dispos.*
574 **1997,** *25*, (1), 116-122.

575 (22) Ricken, B.; Kolvenbach, B. A.; Corvini, P. F. *Ipso*-substitution--the hidden gate to
576 xenobiotic degradation pathways. *Curr. Opin. Biotechnol.* **2015,** *33*, 220-227.

577 (23) Tezuka, Y.; Takahashi, K.; Suzuki, T.; Kitamura, S.; Ohta, S.; Nakamura, S.; Mashino, T.
578 Novel metabolic pathways of p-n-nonylphenol catalyzed by cytochrome p450 and estrogen
579 receptor binding activity of new metabolites. *J. Health Sci.* **2007,** *53*, (5), 552-561.

(24) Ohe, T.; Hirobe, M.; Mashino, T. Novel metabolic pathway of estrone and 17beta-estradiol catalyzed by cytochrome P-450. *Drug Metab. Dispos.* **2000,** *28*, (2), 110-112.

(25) Rittle, J.; Green, M. T. Cytochrome P450 Compound I: capture, characterization, and C-H bond activation kinetics. *Science* **2010,** *330*, (6006), 933-937.

(26) Yosca, T. H.; Ledray, A. P.; Ngo, J.; Green, M. T. A new look at the role of thiolate ligation in cytochrome P450. *J. Biol. Inorg. Chem.* **2017,** *22*, (2-3), 209-220.

(27) Ortiz de Montellano, P. R.; De Voss, J. J. In *Cytochrome P450: Structure, Mechanism, and Biochemistry*, 3rd ed.; Ortiz de Montellano, P. R., Ed. Kluwer Academic/Plenum Publishers: New York, 2005; pp 183-230.

(28) Schyman, P.; Lai, W.; Chen, H.; Wang, Y.; Shaik, S. The directive of the protein: how does cytochrome P450 select the mechanism of dopamine formation? *J. Am. Chem. Soc.* **2011,** *133*, (20), 7977-7984.

(29) Ji, L.; Schuurmann, G. Computational biotransformation profile of paracetamol catalyzed by cytochrome P450. *Chem. Res. Toxicol.* **2015,** *28*, (4), 585-596.

(30) Paneth, P. Chlorine kinetic isotope effects on enzymatic dehalogenations. *Acc. Chem. Res.* **2003,** *36*, (2), 120-126.

(31) Dybala-Defratyka, A.; Szatkowski, L.; Kaminski, R.; Wujec, M.; Siwek, A.; Paneth, P. Kinetic isotope effects on dehalogenations at an aromatic carbon. *Environ. Sci. Technol.* **2008,** *42*, (21), 7744-7750.

(32) Jensen, K. P.; Ryde, U. Cobalamins uncovered by modern electronic structure calculations. *Coord. Chem. Rev.* **2009,** *253*, (5-6), 769-778.

(33) Shaik, S.; Cohen, S.; Wang, Y.; Chen, H.; Kumar, D.; Thiel, W. P450 enzymes: their structure, reactivity, and selectivity-modeled by QM/MM calculations. *Chem. Rev.* **2010,** *110*, (2), 949-1017.

(34) Garcia-Melchor, M.; Braga, A. A.; Lledos, A.; Ujaque, G.; Maseras, F. Computational perspective on Pd-catalyzed C-C cross-coupling reaction mechanisms. *Acc. Chem. Res.* **2013,** *46*, (11), 2626-2634.

(35) Li, Y.; Shi, X.; Zhang, Q.; Hu, J.; Chen, J.; Wang, W. Computational evidence for the detoxifying mechanism of epsilon class glutathione transferase toward the insecticide DDT. *Environ. Sci. Technol.* **2014,** *48*, (9), 5008-5016.

(36) Sadowsky, D.; McNeill, K.; Cramer, C. J. Dehalogenation of aromatics by nucleophilic aromatic substitution. *Environ. Sci. Technol.* **2014,** *48*, (18), 10904-10911.

(37) Pati, S. G.; Kohler, H. P.; Pabis, A.; Paneth, P.; Parales, R. E.; Hofstetter, T. B. Substrate and enzyme specificity of the kinetic isotope effects associated with the dioxygenation of nitroaromatic contaminants. *Environ. Sci. Technol.* **2016,** *50*, (13), 6708-6716.

(38) Himo, F. Recent trends in quantum chemical modeling of enzymatic reactions. *J. Am. Chem. Soc.* **2017,** *139*, (20), 6780-6786.

(39) Schecter, A.; Malik, N.; Haffner, D.; Smith, S.; Harris, T. R.; Paepke, O.; Birnbaum, L. Bisphenol A (BPA) in U.S. food. *Environ. Sci. Technol.* **2010,** *44*, (24), 9425-9430.

(40) Im, J.; Loffler, F. E. Fate of Bisphenol A in terrestrial and aquatic environments. *Environ. Sci. Technol.* **2016,** *50*, (16), 8403-8416.

(41) Ji, L.; Schuurmann, G. Computational evidence for alpha-nitrosamino radical as initial metabolite for both the P450 dealkylation and denitrosation of carcinogenic nitrosamines. *J. Phys. Chem. B* **2012,** *116*, (2), 903-912.

(42) Ji, L.; Schuurmann, G. Model and mechanism: N-hydroxylation of primary aromatic amines by cytochrome P450. *Angew. Chem. Int. Ed.* **2013,** *52*, (2), 744-748.

(43) Zhang, J.; Ji, L.; Liu, W. *In Silico* prediction of cytochrome P450-mediated biotransformations of xenobiotics: a case study of epoxidation. *Chem. Res. Toxicol.* **2015,** *28*, (8), 1522-1531.

(44) Kepp, K. P. Heme: From quantum spin crossover to oxygen manager of life. *Coord. Chem. Rev.* **2017,** *344*, 363-374.

(45) Lee, C. T.; Yang, W. T.; Parr, R. G. Development of the Colle-Salvetti correlation-energy formula into a functional of the electron-density. *Physical Review B* **1988,** *37*, (2), 785-789.

(46) Becke, A. D. Density-functional thermochemistry .3. The role of exact exchange. *J. Chem. Phys.* **1993,** *98*, (7), 5648-5652.

(47) Hay, P. J.; Wadt, W. R. Abinitio Effective Core Potentials for Molecular Calculations - Potentials for the Transition-Metal Atoms Sc to Hg. *J. Chem. Phys.* **1985,** *82*, (1), 270-283.

(48) Kumar, D.; de Visser, S. P.; Shaik, S. How does product isotope effect prove the operation of a two-state "rebound" mechanism in C-H hydroxylation by cytochrome P450? *J. Am. Chem. Soc.* **2003,** *125*, (43), 13024-13025.

(49) Porro, C. S.; Kumar, D.; de Visser, S. P. Electronic properties of pentacoordinated heme complexes in cytochrome P450 enzymes: search for an Fe(I) oxidation state. *Phys. Chem. Chem. Phys.* **2009,** *11*, (43), 10219-10226.

(50) Strickland, N.; Harvey, J. N. Spin-forbidden ligand binding to the ferrous-heme group: Ab initio and DFT studies. *J. Phys. Chem. B* **2007,** *111*, (4), 841-852.

(51) Altun, A.; Breidung, J.; Neese, F.; Thiel, W. Correlated Ab Initio and Density Functional Studies on H2 Activation by FeO(.). *J. Chem. Theory Comput.* **2014,** *10*, (9), 3807-3820.

(52) Ogliaro, F.; Harris, N.; Cohen, S.; Filatov, M.; de Visser, S. P.; Shaik, S. A model "rebound" mechanism of hydroxylation by cytochrome P450: Stepwise and effectively concerted pathways, and their reactivity patterns. *J. Am. Chem. Soc.* **2000,** *122*, (37), 8977-8989.

(53) Tao, J.; Perdew, J. P.; Staroverov, V. N.; Scuseria, G. E. Climbing the density functional ladder: nonempirical meta-generalized gradient approximation designed for molecules and solids. *Phys. Rev. Lett.* **2003,** *91*, (14), 146401.

(54) Staroverov, V. N.; Scuseria, G. E.; Tao, J. M.; Perdew, J. P. Comparative assessment of a new nonempirical density functional: Molecules and hydrogen-bonded complexes. *J. Chem. Phys.* **2003,** *119*, (23), 12129-12137.

(55) Perdew, J. P.; Wang, Y. Accurate and simple analytic representation of the electron-gas correlation energy. *Phys Rev B Condens Matter* **1992,** *45*, (23), 13244-13249.

(56) Becke, A. D. Density-functional exchange-energy approximation with correct asymptotic-behavior. *Physical Review A* **1988,** *38*, (6), 3098-3100.

(57) Adamo, C.; Barone, V. Exchange functionals with improved long-range behavior and adiabatic connection methods without adjustable parameters: The mPW and mPW1PW models. *J. Chem. Phys.* **1998,** *108*, (2), 664-675.

(58) Zhao, Y.; Truhlar, D. G. A new local density functional for main-group thermochemistry, transition metal bonding, thermochemical kinetics, and noncovalent interactions. *J. Chem. Phys.* **2006,** *125*, (19), 194101.

(59) Cao, X. Y.; Dolg, M.; Stoll, H. Valence basis sets for relativistic energy-consistent small-core actinide pseudopotentials. *J. Chem. Phys.* **2003,** *118*, (2), 487-496.

(60) Miertus, S.; Scrocco, E.; Tomasi, J. Electrostatic interaction of a solute with a continuum - a direct utilization of abinitio molecular potentials for the prevision of solvent effects. *Chem. Phys.* **1981,** *55*, (1), 117-129.

(61) Ogliaro, F.; de Visser, S. P.; Cohen, S.; Kaneti, J.; Shaik, S. The experimentally elusive oxidant of cytochrome P450: a theoretical "trapping" defining more closely the "real" species. *ChemBioChem* **2001,** *2*, (11), 848-851.

(62) Marenich, A. V.; Cramer, C. J.; Truhlar, D. G. Universal solvation model based on solute electron density and on a continuum model of the solvent defined by the bulk dielectric constant and atomic surface tensions. *J. Phys. Chem. B* **2009,** *113*, (18), 6378-6396.

(63) Grimme, S. Semiempirical GGA-type density functional constructed with a long-range dispersion correction. *J. Comput. Chem.* **2006,** *27*, (15), 1787-1799.

679 (64) Williams, P. A.; Cosme, J.; Vinkovic, D. M.; Ward, A.; Angove, H. C.; Day, P. J.; Vonrhein,
680 C.; Tickle, I. J.; Jhoti, H. Crystal structures of human cytochrome P450 3A4 bound to metyrapone
681 and progesterone. *Science* **2004,** *305*, (5684), 683-686.

682 (65) Frisch, M. J., et al., Gaussian 09, revision D.01, Gaussian, Inc.: Wallingford, CT, 2013. See
683 Supporting Information.

684 (66) Shaik, S.; Kumar, D.; de Visser, S. P. Valence bond modeling of trends in hydrogen
685 abstraction barriers and transition states of hydroxylation reactions catalyzed by cytochrome P450
686 enzymes. *J. Am. Chem. Soc.* **2008,** *130*, (31), 10128-10140.

687 (67) Lonsdale, R.; Harvey, J. N.; Mulholland, A. J. Inclusion of Dispersion Effects Significantly
688 Improves Accuracy of Calculated Reaction Barriers for Cytochrome P450 Catalyzed Reactions. *J.*
689 *Phys. Chem. Lett.* **2010,** *1*, (21), 3232-3237.

690 (68) Kolvenbach, B.; Schlaich, N.; Raoui, Z.; Prell, J.; Zuhlke, S.; Schaffer, A.; Guengerich, F.
691 P.; Corvini, P. F. Degradation pathway of bisphenol A: does *ipso* substitution apply to phenols
692 containing a quaternary alpha-carbon structure in the para position? *Appl. Environ. Microbiol.*
693 **2007,** *73*, (15), 4776-4784.

694 (69) Kohler, H. P. E.; Gabriel, F. L. P.; Giger, W. *Ipso*-substitution - A novel pathway for
695 microbial metabolism of endocrine-disrupting 4-nonylphenols, 4-alkoxyphenols, and bisphenol A.
696 *Chimia* **2008,** *62*, (5), 358-363.

697 (70) Gabriel, F. L.; Cyris, M.; Giger, W.; Kohler, H. P. *Ipso*-substitution: a general biochemical
698 and biodegradation mechanism to cleave alpha-quaternary alkylphenols and bisphenol A. *Chem.*
699 *Biodivers.* **2007,** *4*, (9), 2123-2137.

(71) Schmidt, J.; Kotnik, P.; Trontelj, J.; Knez, Z.; Masic, L. P. Bioactivation of bisphenol A and its analogs (BPF, BPAF, BPZ and DMBPA) in human liver microsomes. *Toxicol. In Vitro* **2013,** *27*, (4), 1267-1276.

(72) Anslyn, E. V.; Dougherty, D. A. *Modern Physical Organic Chemistry*. University Science Books: Sausalito, CA, 2006.

(73) Drug Metabolism Prediction. In Kirchmair, J., Ed. John Wiley & Sons: Weinheim, **2014**.

(74) Kirchmair, J.; Goller, A. H.; Lang, D.; Kunze, J.; Testa, B.; Wilson, I. D.; Glen, R. C.; Schneider, G. Predicting drug metabolism: experiment and/or computation? *Nat. Rev. Drug Discov.* **2015,** *14*, (6), 387-404.

(75) Meerts, I. A.; Letcher, R. J.; Hoving, S.; Marsh, G.; Bergman, A.; Lemmen, J. G.; van der Burg, B.; Brouwer, A. In vitro estrogenicity of polybrominated diphenyl ethers, hydroxylated PDBEs, and polybrominated bisphenol A compounds. *Environ. Health Perspect.* **2001,** *109*, (4), 399-407.

(76) Connor, K.; Ramamoorthy, K.; Moore, M.; Mustain, M.; Chen, I.; Safe, S.; Zacharewski, T.; Gillesby, B.; Joyeux, A.; Balaguer, P. Hydroxylated polychlorinated biphenyls (PCBs) as estrogens and antiestrogens: Structure-activity relationships. *Toxicol. Appl. Pharmacol.* **1997,** *145*, (1), 111-123.

(77) Ricken, B.; Corvini, P. F. X.; Cichocka, D.; Parisi, M.; Lenz, M.; Wyss, D.; Martinez-Lavanchy, P. M.; Mueller, J. A.; Shahgaldian, P.; Tulli, L. G.; Kohler, H.-P. E.; Kolvenbach, B. A. *ipso*-Hydroxylation and subsequent fragmentation: a novel microbial strategy to eliminate sulfonamide antibiotics. *Appl. Environ. Microbiol.* **2013,** *79*, (18), 5550-5558.

721

722

723

724 **TOC GRAPHIC**

725

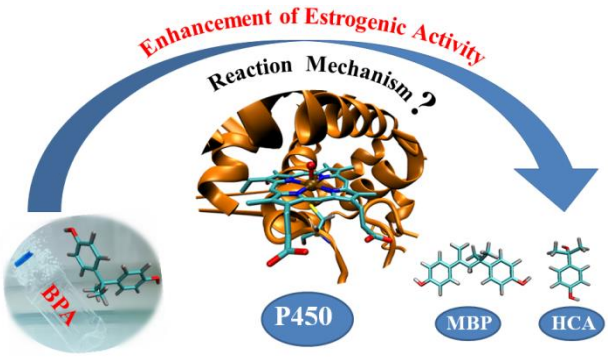

726

727